Cyclic martensitic phase transformation in multi-variant mono-crystals at finite strains using UMAT

Erwin Stein and Gautam Sagar

Institute of Mechanics and Computational Mechanics (IBNM)
Leibniz University of Hannover, Appelstr. 9A, D-30167 Hannover, Germany

e-mail: stein@ibnm.uni-hannover.de, sagar@ibnm.uni-hannover.de

Abstract: Numerical validation of a mico-macro material model for solid-solid martensitic phase transformation (PT) of multi-variant mono-crystals at finite strains with comparisons to linearized strains is presented, using reliable experimental data. The material and numerical models are based on work by Govindjee and Miehe (2001) and by Stein and Zwickert (2006) at linearized strains and extended to finite strains by Stein and Sagar (submitted 2006). In the above mentioned works, C^1-continuous thermo-mechanical micro-macro PT-theory using Bain's principle is presented by a unified Lagrangian functional including phase evolution equations with mass conservation and quasi-convexification of energy wells.

Iterative time-integration of the phase transformation evolution equation was programmed in C++ and implemented into Abaqus via UMAT-interface. In case of non-linear material model with finite strains Abaqus requires Jaumann rate of Cauchy stresses for current tangent (stiffness). Computations were done using 3D-hexahedral and 3D tetrahedral B-bar elements. Numerical validation of the used micro-macro material models are presented by comparing numerical results with experimental data supplied by Xiangyang et al. (2000) for $Cu_{82}Al_{14}Ni_4$ monocrystals, at both, quasiplastic and superelastic PTs. The zigzag type experimental stress-strain curve, called 'yield tooth', for quasiplastic PT within the loading process of a uniaxial tension specimen is numerically approximated sufficiently good by the computationally obtained averaged curve which could not be achieved with linearized kinematics.

Keywords: Shape memory alloys, Finite strain, Martensitic phase transformation, Implementation, Validation.

1. Problem description

The specific feature of shape memory alloys with martensitic phase transformations (PTs) is the ability to 'remember' their initial state. After elastic deformation and subsequent quasiplastic PT (at a critical state stress at subcritical temperature) a shape memory alloy (SMA) will only recover its old shape after unloading if a second (higher) critical temperature is reached by heating (shape memory effect, SME). Phase transformation stains usually are up to 15%, such that finite strain theory is adequate. There are some promising macro and micro-macro constitutive material

models available for quasiplastic and superelastic martensitic phase transformation cycles of poly- and mono- crystalline metal alloys. In case of mono-crystalline alloys a major theoretical and numerical difficulty is the convexification of the of the energy wells, fig. 1a, for multiple phase variants with a phase vector, which is not required for poly- crystalline alloys. In this paper, implementation and numerical validation of a micro-macro PT material model for solid-solid martensitic phase transformation of multi-variant mono-crystals at finite strains are presented with comparison to linearized strains.

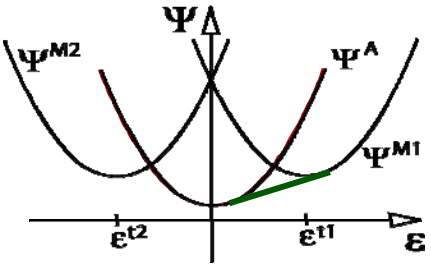

Figure 1a. Convexification of energy wells for multiple PT variants.

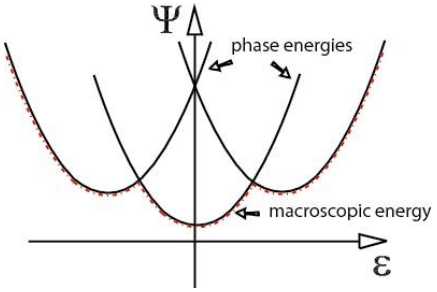

Figure 1b. Macroscopic energy (marked line) as a connection of minimal energy wells of phase variants.

2. Mathematical modeling

The unified micro-macro PT material model (Govindjee and Miehe, 2001) and in a refined form (Stein and Zwickert, 2006), both at small strains for multiple phase variants, is extended to finite strain kinematics (Stein and Sagar, 2006). The term 'unified model' denotes the extension of the Helmholtz free energy to a Lagrangian functional, as introduced by Patoor et al. (1995) for a two-phase material. This PT-model is based on the assumption by Ball and James (1987) that the macroscopic free strain energy, fig. 1b, of a crystal corresponds to the minimum of the energies of all possible variants.

The deformation model is based on the multiplicative decomposition of the total deformation gradient into elastic and transformation part, eq. 1, (Stein and Sagar, 2006), (Levitas et. al, 2001). Actual plastic deformations are not considered. The Neo-Hookean hyperelastic material model, eq. 5, including mass conservation with respect to phase fractions, eq. 32-33, and convexified free energy, eq. 4, is used for mono-crystalline shape memory alloys in order to get the C^1-continuous constitutive model at large strains where transformation strains during phase transition can reach up to 15%.

This is followed by the extension of the free energy by a Langragian functional, eq. 17, that accounts for kinematic constraints, eq. 18, of the material with martensitic PT cycles subjected to cooling, mechanical loading and heating. This generalized representation yields the canonical derivatives of this functional: stresses, eq. 19, phase transformation vector and vector of thermodynamical forces, eq. 20. The PT criteria, eq. 23, and an evolution law, eq. 26, for internal variables (ξ: phase transformation vector, bounded by mass conservation, λ: strain controlled load factor, δ: Lagrangian parameter for mass conservation and γ: partial phase energy vector) of the model complete the system of constitutive equations.
In order to separate mathematical theory from computational aspects a summary of PT-model formulae is presented in Box 1. For further details see (Stein and Sagar, 2006).

Box 1. Summary of PT-model equations.

Multiplicative decomposition of the total material deformation gradient into elastic $\mathbf{F}^e$, transformation $\mathbf{F}^t$ and plastic $\mathbf{F}^p$ parts

$$\mathbf{F} = \mathbf{F}^e\,\mathbf{F}^t\,\mathbf{F}^p;\ \mathbf{F}^P \equiv \mathbf{I} \tag{1}$$

Elastic left Cauchy-Green tensor for phase i with transformation stretch tensor $\mathbf{U}_i^t = \mathbf{v}_i^t$

$$\mathbf{b}_i^e = \mathbf{F}\left(\mathbf{U}_i^{t\,2}\right)^{-1}\mathbf{F}^T \tag{2}$$

Quasi-convexified free energy for linearized elasticity

$$\Psi(\varepsilon,\xi) = \xi\cdot\psi(\varepsilon) + \Psi_{LS}^M(\tilde{\varepsilon}^t,\xi) \tag{3}$$

Quasi-convexified free energy at finite strains

$$\Psi(\mathbf{b},\xi) = \xi\cdot\psi(\mathbf{b}) + \Psi_{FS}^M(\mathbf{b}^t,\xi) \tag{4}$$

Elastic energy for phase i from hyperelastic material model

$$\psi_i^{el}(\mathbf{b}_i^e, J_i^e) = W_i(J_i^e) + \overline{W_i}\,(\overline{\mathbf{b}_i^e}), \tag{5}$$

$$W_i(J_i^e) := \tfrac{1}{2}\kappa\left[\ \tfrac{1}{2}(J_i^{e2}-1) - \ln J_i^e\ \right],$$

$$\overline{W_i}\,(\overline{\mathbf{b}_i^e}) := \tfrac{1}{2}\mu\,(\,\mathrm{tr}[\overline{\mathbf{b}_i^e}]-3) \tag{6}$$

$$\overline{\mathbf{b}_i^e} := J_i^{e-2/3}\,\mathbf{F}_i^e\,\mathbf{F}_i^{e\,T} \equiv J_i^{e-2/3}\,\mathbf{b}_i^e$$

$$J_i^e = \det\mathbf{F}_i^e = \det\mathbf{F}\cdot\det\mathbf{F}_i^{t-1} = \det\mathbf{F}\cdot\det\left(\mathbf{v}_i^t\right)^{-1} \tag{7}$$

Chemical free energy for n-phase material

$$\psi^{ch} = \sum_{i=1}^{n} \psi_i^{ch} = \sum_{i=1}^{n} \left[\rho l_i \left(\frac{\theta - \theta_0}{\theta_0} \right) + \rho c_i \theta \left(1 - \log\left(\frac{\theta}{\theta_0} \right) \right) \right] \tag{8}$$

l_i - latent heat of the i-th phase, c_i - specific heat capacity of the i-th phase, ρ - mass density, θ - temperature, and θ_0 - reference temperature

$$\Psi_{LS}^{M}(\tilde{\varepsilon}^t, \xi) = -\frac{1}{2} \sum_{i=1}^{n} \xi_i \, \tilde{\varepsilon}_i^t : \mathbb{C} : \tilde{\varepsilon}_i^t + \frac{1}{2} \sum_{i=1}^{n} \sum_{j=1}^{n} \xi_i \, \xi_j \, \tilde{\varepsilon}_i^t : \mathbb{C} : \tilde{\varepsilon}_j^t \tag{9}$$

$\tilde{\varepsilon}_i^t = \tilde{\mathbf{R}} \, \varepsilon_i^t \, \tilde{\mathbf{R}}^T$, $\mathbb{C}$ - linear elasticity tensor, $\tilde{\mathbf{R}}$ - crystal orientation matrix, ε_i^t - linearized transformation strain of phase i

$$\varepsilon_i^t = \frac{1}{2}\left(\mathbf{U}_i^{t\ 2} - 1 \right) \approx \mathbf{U}_i^t - 1 \tag{10}$$

Free energy of mixing at finite strains

$$\Psi_{FS}^{M}(\mathbf{b}^t, \xi) \approx -\sum_{i=1}^{n} \xi_i \, \psi_i^t(\mathbf{b}_i^t, J_i^t) + \sum_{i=1}^{n} \sum_{j=1}^{n} p_{ij}(\mathbf{b}_i^t, \mathbf{b}_j^t) \, \xi_i \, \xi_j \, \sigma_i^t(\mathbf{b}_i^t, J_i^t) : \left[\frac{1}{2} ln(\mathbf{b}_j^t) \right] \tag{11}$$

$p_{ij} \in \mathbb{R}, i \neq j$ account for the non-linearity of the stress-strain function

$$p_{ij} \, \sigma_i^t(\mathbf{b}_i^t) : \frac{1}{2} ln(\mathbf{b}_j^t) = \int_{\mathbf{b}_j^{*t}=1}^{\mathbf{b}_j^t} \sigma_i^t(\mathbf{b}_i^{*t}) : d\left(\frac{1}{2} ln(\mathbf{b}_j^{*t}) \right) \tag{12}$$

$$\text{with} \quad p_{ij} \geq \frac{1}{2} \ \text{for} \ \sigma_{kl\,i} \geq 0, b_{kl\,j} \geq 0$$

$$p_{ij} \approx \frac{1}{2} \quad \text{for} \ \sigma_{kl\,i} \leq 0, b_{kl\,j} \leq 0 \ \text{where} \ b_{kl\,j} \approx \mp 0.15 \tag{13}$$

$$\text{and} \ p_{ij} \leq \frac{1}{2} \ \text{for different signs} \tag{14}$$

Approximated free energy of mixing for a 2-phase system (1 means austenite, 2 means martensite)

$$\Psi_{FS}^{M}(\mathbf{b}^t,\xi) \approx -\xi_2\ \psi_2^t(\mathbf{b}_2^t, J_2^t) + \xi_2\ \xi_2\ \psi_2^t(\mathbf{b}_2^t, J_2^t)\,, \tag{15}$$

because

$$\mathbf{b}_1^t = 1, \frac{1}{2} ln(\mathbf{b}_1^t) = 0 \text{ and } \psi_1^t(\mathbf{b}_1^t, J_1^t) = 0 \tag{16}$$

Lagrangian functional

$$L(\mathbf{b},\xi,\gamma,\delta) = \Psi(\mathbf{b},\xi) - \gamma\cdot\xi + \delta(\mathbf{e}^*\cdot\xi - 1) \tag{17}$$

Kuhn-Tucker conditions

$$\gamma \geq 0; -\xi \leq 0\,; \gamma\cdot\xi = 0 \text{ with } \xi = \sum_{i=1}^{n} \xi_i \mathbf{e}_i \in P^{n-1} \tag{18}$$

Cauchy stress, including PT process

$$\begin{aligned}\sigma^*(\mathbf{b}^e,\xi) &= \frac{2}{J^e}\,\mathbf{b}^e\,\frac{\partial L}{\partial \mathbf{b}^e} = \frac{2}{J^e}\,\mathbf{b}^e\,\frac{\partial \Psi(\mathbf{b},\xi)}{\partial \mathbf{b}^e} \\ &= \sum_{i=1}^{n}\ \frac{2}{J_i^e}\,\mathbf{b}_i^e\left(\xi_i\frac{\partial \psi_i(\mathbf{b})}{\partial \mathbf{b}_i^e} + \frac{\partial \Psi_i(\mathbf{b}_i^t,\xi_i)}{\partial \mathbf{b}_i^e}\right) \\ &= \sum_{i=1}^{n}\ \xi_i\,\sigma_i(\mathbf{b}_i^e, J_i^e)\end{aligned} \tag{19}$$

Thermodynamical driving force

$$\mathbf{f} = -\frac{\partial L}{\partial \xi} = -\psi(\mathbf{b}) - \partial_{\xi}\Psi_{FS}^{M}(\mathbf{b}^t,\xi) + \gamma - \delta\mathbf{e}^* = 0 \tag{20}$$

Local dissipation inequality

$$D = \mathbf{f}\cdot\dot{\xi} \geq 0 \tag{21}$$

Local maximum dissipation principle

$$\mathbf{f}\cdot\dot{\xi} \rightarrow \text{Max} \tag{22}$$

PT condition

$$\phi = \|\mathbf{f}\| - f_c \leq 0, \quad f_c - \text{critical driving force} \tag{23}$$

Local Lagrangian functional for the stationary dissipation principle, fulfilling the PT condition

$$\Pi(\mathbf{f}, \lambda) = -D + \lambda\phi \longrightarrow \text{stat} \tag{24}$$

Kuhn-Tucker conditions for the saddle point problem

$$\lambda \geq 0, \phi \leq 0, \text{ and } \lambda\phi = 0 \tag{25}$$

PT-flow rule, normality rule

$$\partial_{\mathbf{f}}\Pi = -\dot{\xi} + \lambda\,\partial_{\mathbf{f}}\psi = 0 \Rightarrow \dot{\xi} = \lambda\partial_{\mathbf{f}}\phi \tag{26}$$

3. Time integration

The constitutive model is strain and temperature controlled. It is assumed that at a time t_n the entire state of the material is known and has to be updated to time t_{n+1}. Backward Euler method is used for time integration. Constitutive equations for time integration with constraints are presented in Box 2. For further details see (Stein and Sagar, 2006), (Stein and Zwickert, 2006), (Govindgee and Miehe, 2001).

Box 2. Numerical integration of PT-flow rule.
Summary of discrete equations to be solved at t_{n+1}.

Time-invariant driving force $\mathbf{f}$ has to fulfill the condition

$$\mathbf{f} + \psi(\mathbf{b}) - \gamma + \partial_{\xi}\Psi_{FS}^{M}(\mathbf{b}^{t}, \xi) + \delta\mathbf{e}^{*} = 0 \tag{27}$$

Local convex phase transformation criteria

$$\phi(\mathbf{f}^{tr}) \begin{cases} \leq 0 & \Rightarrow \quad \text{step } \Delta\lambda \text{ is elastic} (28) \\ \geq 0 & \Rightarrow \quad \text{PT takes place in this step } \Delta\lambda \end{cases} \tag{29}$$

Kuhn-Tucker conditions

$$\Delta\lambda\phi = 0, \Delta\lambda \geq 0, \text{ with incremental } \Delta\lambda = \Delta t\lambda \tag{30}$$

Discrete evolution equation of the phase fraction vector

$$\xi - \xi_n - \Delta\lambda\partial_{\mathbf{f}}\phi = 0 \tag{31}$$

Polytope constraint

$$\mathbf{e}^* \cdot \xi - 1 = 0, \text{ mass conservation condition} \tag{32}$$

$$-\xi_i \le 0, \text{ positiveness of the phase fractions} \tag{33}$$

$$-\gamma \cdot \xi = 0, \text{ first Kuhn} - \text{Tucker condition} \tag{34}$$

$$\gamma_i \ge 0, \text{ second Kuhn} - \text{Tucker condition} \tag{35}$$

Global tangent operator for every Gauss integration point

Variation of total Cauchy stress

$$\delta\sigma^* = \sum_{i=1}^{n} \mathbb{C}_i^{alg\,o} : \delta\mathbf{d} = \sum_{i=1}^{n} \left(\mathbb{C}_i : \delta\mathbf{d} \right) - \sum_{i=1}^{n} \sum_{i=1}^{n} \left(\mathbb{C}_{ij}^{PT} : \delta\mathbf{d} \right) \tag{36}$$

with the tangent moduli

$$\mathbb{C}_{ij}^{PT} = \mathbf{D}_{ij} \cdot \left[\sigma_i(\mathbf{b}_i^e) \otimes \sigma_j(\mathbf{b}_j^e) \right], \tag{37}$$

$$\mathbf{D}_{ij} = \delta_{\mathbf{f}}\phi \otimes \mathbf{v} + \Delta\lambda\delta_{\mathbf{ff}}\, 2\phi \cdot \mathbf{v} \tag{38}$$

$\mathbf{v}$ is the first n values of the (n+m+1) th block of $\mathbf{K}^{-1}$ and $\mathbb{C}_i$ is spatial elasticity tensor of i-th phase

---

4. Comparisons of finite strain PT-theory with linearized strain

- In case of linear kinematics, each phase (austenite or a martensitic phase) has the same elasticity tensor, eq. 9, which remains constant throughout the process whereas in case of finite strain kinematics each phase has its own elasticity tensor, eq. 36, which is a function of deformation gradient and thus changing during the PT-process.
- The convexified energy for free energy of mixing within linear kinematics, eq. 3, is extended to the corresponding hyperelastic energy with finite strains, eq. 4. The bounding property of energy of mixing is treated in eq. 11 - 14.

5. Implemetation in Abaqus via UMAT

Due of its open architecture, Abaqus UMAT-interface was chosen for the implementation of the material models given in Box 1 and in Box 3. It is easy to implement the general material model with linearized strains in Abaqus via UMAT, but it is rather complicated to implement the material model with finite strains via UMAT and to achieve quadratic convergence in regular cases.

As the stationary material model has finite strain kinematics and hyperelastic free energy function, the non-linear implementation of UMAT is needed; it requires tangent moduli (stiffnesses) in current configuration which is associated with the Jaumann rate of Cauchy stress. In index notation the spatial tangent related to Jaumann rate of Cauchy stress is given in Box 3, eq. 39, which is not included in Abaqus manuals. Quadratic convergence of Abaqus finite elements can only be achieved by using the objective Jaumann rate even in cases of rate independent materials. The analytical tangent and even numerical tangent are insufficient for it see (Sagar and Stein, 2006).

The algorithms for the material equations, Box 1 and Box 3, are programmed in C++ and coupled by Abaqus via UMAT. The expression ‘extern "C" ’ has to appear before the declaration of the C++ subroutine. For using a 'character string' which is passed from FORTRAN to the C++ routine one has to implement a function that converts a FORTRAN CHARACTER string into a C++ string which are not compatible. In order to reach compatibility, functions callable for FORTRAN must be declared as

... FOR_NAME(subnam,SUBNAM)(...).

The FOR_NAME macro allows system-dependent handling of function names.

Depending on the ABAQUS version and the installed compilers the UMAT subroutine has to be compiled by a command contained in the data file abaqus_X.env (with version number X) located in the ABAQUS installation directory under … \ Version \ site. For thee version 6.4 and the compilers Visual C++ 6.0 and Visual Fortran 6 the UMAT has to be compiled with

“ ‘cl /c /nologo /W0 /MD /TP /DNDEBUG /DWIN32 /DTP_IP /D_CONSOLE /DNTI /DFLT_LIC /DOL_DOC /D__LIB__ /DHKS_NT /DFAR= /D_WINDOWS /O1 /I%I’ “.

Furthermore, two additional classes 'vector' and 'matrix' are implemented in which the mathematical operators - like matrix multiplication - are defined. It makes the calculations within the material routine clearer and helps to avoid mistakes in the programming.

In order to implement the finite strain micro-macro PT-model into Abaqus via UMAT, the subroutine UMAT is called at the beginning of each (process) time steps for every integration point of the spatial finite elements in ABAQUS. Among many further variables, STRAIN (total strain), DSTARIN (strain increment), DDSDDE (material tangent) and STATEV (here the phase fractions) are passed to UMAT for the implementation of PT model, (Stein and Sagar, 2006).

Box 3. Formulation for implementation in Abaqus via UMAT-interface

Index notation of the spatial tangent related to Jaumann rate of Cauchy stress

$$\tilde{c}^{abcd} := \overset{\nabla}{c}{}^{abcd}/J = [c^{abcd} + \delta^{ac}\tau^{bd} + \tau^{ac}\delta^{bd}]/J \tag{39}$$

Implementation of the Neo-Hookean hyperelastic model via UMAT

Total free strain energy of two parameter model

$$\psi(I_c, J) = g(J) + \frac{1}{2}\mu(I_c - 3) \tag{40}$$

$$g(J) = c(J^2 - 1) - d\ln J - \mu \ln J \tag{41}$$

$$I_c = trace(\mathbf{C}), c = \Lambda/4, d = \Lambda/2 \tag{42}$$

$\mathbf{C}$ is left Cauchy-Green tensor, with $c > 0$, $d > 0$. Λ and μ are Lamé parameters for linearized strain where μ is shear modulus.

6. Examples

6.1 Convergence tests

A Neo-Hookean 2-parametric material model, eq. (40-42), non-linear elastic material with a chosen free energy function was implemented in Abaqus and tested on a simple but significant problem, fig. 2.

A cube with edges of unit length '1' is chosen for the example, fig. 2. The left face, ABCD of the cube is fixed in X direction (as direction 1), the bottom face, ADHE of the cube is fixed in the Y direction (as direction 2) and the back face, ABFE is fixed in Z direction (as direction 3). Displacement-controlled numerical tests with fixed time increments are presented. Equal displacements in all three directions are applied at corner 'G' (X = Y = Z = '1'). The material parameters for the computations are obtained from the chosen Young's modulus, E = 7 MPa, and Poisson's ratio for nearly incompressible material, υ = 0.4999 at linearized strains.
B-bar linear hexahedral and B-bar linear tetrahedral elements are used. All the 3-D elements in Abaqus were tested in (Sagar and Stein, 2006).

The goal of tests was the classification of the rates of convergence for iterative solutions in regular cases, especially the intended quadratic convergence of appropriate iterative solvers for finite element discretization. The default value of convergence tolerance, 5.0E-03, is taken from Abaqus.

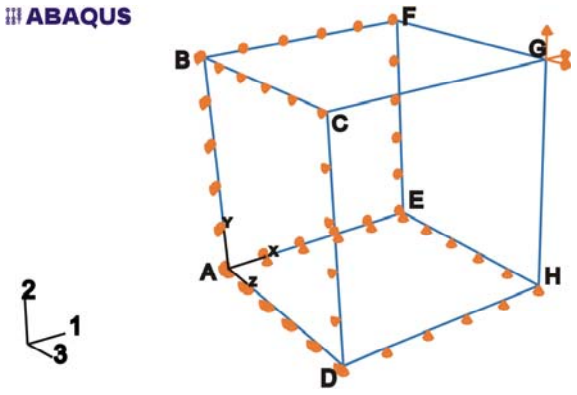

Figure 2. Unit cube in reference configuration with boundary conditions and applied loads.

Test 1: 8-node linear brick, C3D8 (hexahedral) B-bar element is used for the computation. The cube is discritized by 5 x 5 x 5 = 125 elements. For the applied displacements $u_x = u_y = u_z = 0.5$ (geometric engineering strain $\varepsilon_x = \varepsilon_y = \varepsilon_z = 50\%$), quadratic rate of convergence is achieved.

Test 2: 4-node linear tetrahedral C3D4 B-bar element is used for the computation. The cube is discritized by imposing 5 seeds (nodes) at all the edges. For the applied displacements $u_x = u_y = u_z = 0.5$ (geometric engineering strain $\varepsilon_x = \varepsilon_y = \varepsilon_z = 50\%$), quadratic rate of convergence is achieved.

6.2 Validation of PT-model

The validation of the PT model for shape memory effect (SME) is carried out with experimental data supplied by Xiangyang et al. (2000) with specimen made from $Cu_{82}Al_{14}Ni_{14}$ monocrystals, using linear 3D finite elements. The experimental details given in (Xiangyang et al., 2000) and material data are available in (Stein and Zwickert, 2006), (Sagar and Stein, 2006). For numerical comparison only the effective part (gauge length 25 mm) of tension specimen is analyzed. The finite element model is 25 mm long, 4mm wide and 1 mm thick and used for computation with the 3D B-bar hexahedral element. Computation is done in three steps, in step 1, the strain is increased as displacement controlled load, in step 2, strain is decreasing by elastic unloading, and in step 3, heating is applied.

The automatic time stepping is chosen from Abaqus for the whole cyclic process. The spatial FE-discretization was carried out with 176 linear 8-node B-bar hexahedral elements of the type C3D8 in ABAQUS.

Comparison of experimental stress-strain behavior of SME-specimen with the numerically obtained data at linearized PT strains is shown in fig. 3a and comparison of numerical stress-strain behavior at finite PT strains with such for linearized strains is presented in fig. 3b, both for full PT

cycles of SME. The experimental zigzag type stress-strain curve shows decreases after reaching a first critical stress, accompanied with an abrupt growth of strain and followed again by an increase of stress, a phenomenon often addressed as 'yield tooth'. Next, stress – strain grows again linearly with almost the same gradient as in the forgoing linear elastic path. This process repeats several times during PT.

The experimental results for quasiplastic PT are numerically approximated by the computationally obtained smoothed curve which could not be achieved with linearized kinematics. Fig.3a,b shows that PK1-transformation-stress with non-linear kinematics is 1.6 % less than with linear kinematics, and approximately 2 % less than the experimentally measured stress. The residual PT strains after elastic unloading for non-linear kinematics are smaller by 3 % than those with linear strain.

Fig. 4a shows the distribution of austenite (d.o.a) at start of loading process as well as at the end of heating process. Fig. 4b shows d.o.a at 25% of total loading, fig. 4c shows d.o.a at the end of total loading, fig. 4d d.o.a at the end of elastic unloading, and fig. 4e shows d.o.a at 58% of heating. As there is only elastic unloading the distribution of austenite phase is same at the end of loading and at the end of elastic unloading. It is observed that after heating the SME-specimen forms back to 100% austenite that correctly simulates the theory. Fig. 4f shows the full PT-cycle (loading - elastic unloading - heating) of quasiplastic PT for SME.

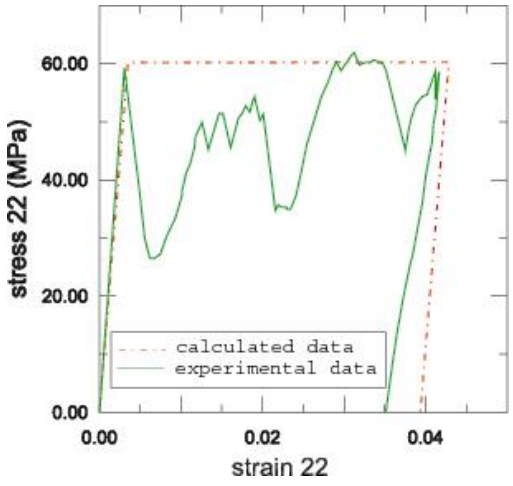

Figure 3a. Engineering stress-strain curve of SME specimen; experimental and computed data with linearized (Stein and Zwickert 2006) $P_{exp.}$ = 58 Mpa, P_{LS} = 57.79 Mpa

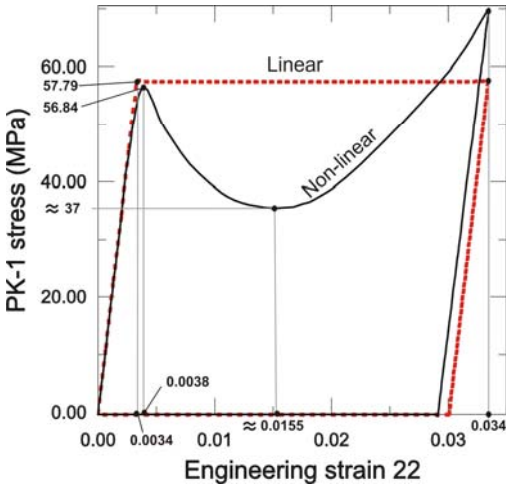

Figure 3b. Engineering stress-strain curve of SME specimen; computed data with linearized strain P_{LS} = 57.79 Mpa and finite strains P_{FS} = 56.84 Mpa

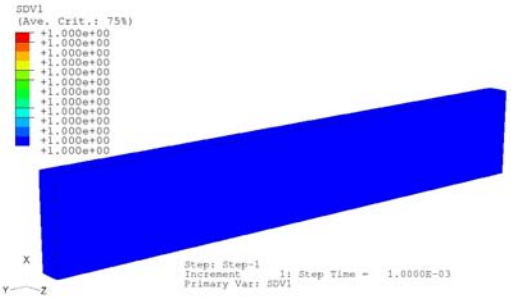

(a) At the beginning of process in step 1 (after 1st displacement increment) and at the end of step 3, **(A)**

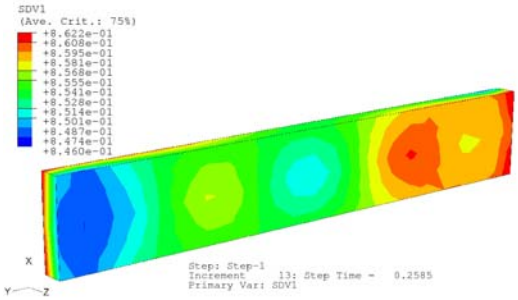

(b) In step 1 at 25% of total deformation, **(A->M)**

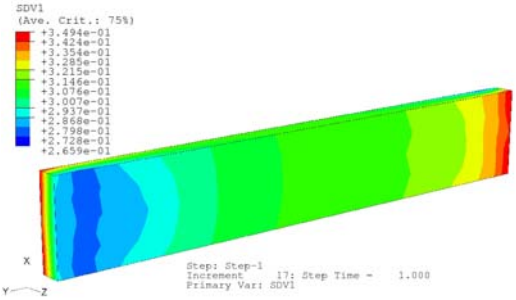

(c) At the end of step 1 (after 100% loading), **(A,M)**

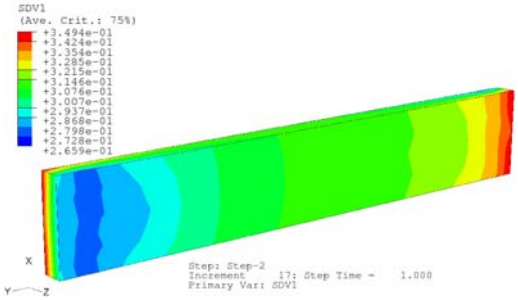

(d) At the end of step 2 (after elastic unloading), **(A,M)**

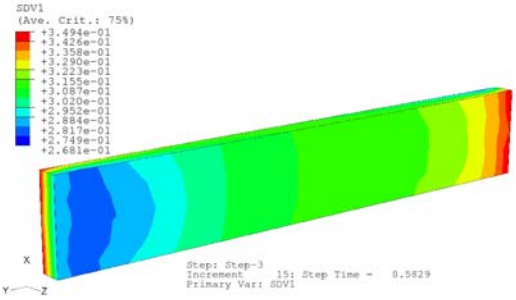

(e) Recovery of austenite, in step 3 after 58% of heating, **(M->A)**

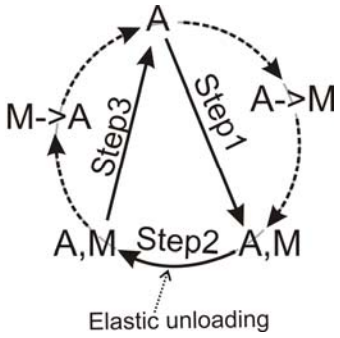

(f) Full PT-cycle

Figure 4. History of the austenite phase fraction in the case of SME

7. Conclusions

- Theoretical and computational extension of the generalized micro-macro PT-model to finite strains of monocrystals shows similar algorithmic structure with the linear theory but needs extra theoretical and algorithmic efforts to implement in Abaqus.
- UMAT interface of Abaqus requires Jaumann rate of Cauchy stress, for quadratic convergence, but only for the hyperelastic terms of the related tangent moduli, eq. 36; this rate is not required for the mixed PT terms, eq. 37, because PT equations are already given in incremental form.
- The zigzag type experimental stress-strain curve within the loading process, called 'yield tooth', is numerically approximated with finite strain theory by an averaged curve which could not be achieved with linearized strain theory.

8. References

1. Ball, J., and R. James, "Fine phase mixtures as minimizers of energy," Archive for Rational Mechanics and Analysis, vol. 100, pp. 13–52, 1987.

2. Govindjee, S., and C. Miehe, "A multi-variant martensitic phase transformation model: formulation and numerical implementation," Computer Methods in Applied Mechanics and Engineering, Vol. 191, pp. 215-238, 2001.

3. Levitas, V.I., A. V. Idesman, and E. Stein, "Shape memory alloys: micromechanical modeling and numerical analysis of structure," Journal of Intelligent Material Systems and Structures 10(12), pp. 983-996, 2001.

4. Patoor, E., A. Eberhardt, and M. Berveiller, "Micromechanical modelling of superelasticity in shape memory alloys," Journal de Physique IV C8-5, pp. 277-292, 1995.

5. Sagar, G., and E. Stein, "Implementation of a non-linear elastic material model with a free energy function in Abaqus 6.4 via UMAT," Proceedings in 18. Deutschsprachige ABAQUS Benutzerkonferenz, Erfurt, 15 pages, 2006.

6. Stein, E., and G. Sagar, "Theory and finite element computation of cyclic martensitic phase transformation with finite strain using UMAT", submitted to International Journal for Numerical Methods in Engineering, 28 pages, 2006.

7. Stein, E., and O. Zwickert, "Theory and finite element computations of a unified cyclic phase transformation model for monocrystalline materials at small strain," International Journal of Computational Mechanics, online printed first, 17 pages, 2006.

8. Xiangyang, Z., S. Quingping, and Y. Shouwen, "A non-invariant plane model for the interface in CuAlNi single crystal shape memory alloys," Journal of the Mechanics and Physics of Solids, vol. 48, pp. 2163-2182, 2000.